2022

Flow characteristics of hydraulically fractured granite rocks under high temperature

Gnamani Pabasara P. Wanniarachchige
University of Wollongong, pabasara@uow.edu.au

Ranjith Pathegama Gamage
Monash University

FLOW CHARACTERISTICS OF HYDRAULICALLY FRACTURED GRANITE ROCKS UNDER HIGH TEMPERATURE

Kumari W.G.P.[1] and Ranjith P.G.[2]

ABSTRACT: Hydraulic fracturing technique, which is widely used to enhance the permeability of tight geological formations, has been employed to stimulate unconventional geothermal systems. However, these reservoirs are accompanied by high in-situ stresses and large geothermal gradients. Therefore, it is important to understand the hydraulic fracturing process and the respective permeability enhancement under extreme temperature and pressure conditions. Therefore, the aim of the present study is to understand the effect of flow performance of hydraulically fractured granite under high temperature and pressure conditions. A series of flow-through experiments were conducted on granite specimens which were hydraulically fractured under 60 MPa confining pressure and two temperature conditions: room temperature and 300 °C. Corresponding influence on rock microstructure was studied using high-resolution CT imaging with the IMBL facility of Australian Synchrotron. Based on the experimental results, it was found that one single fracture is induced at room temperature. However, a perforated zone with multiple inter-crystalline cracks is induced in the wellbore zone under the high-temperature fracturing process. Therefore, the measured permeability was almost one order higher in the sample hydraulically fractured under high temperature up to 20 MPa confining pressure. Further, it was identified that the fracture permeability and the fluid discharge were strongly stressed dependent.

INTRODUCTION

For a successful reservoir stimulation, it is essential to understand reservoir geomechanics, including in situ stress and temperature condition, reservoir rock properties, presence of natural fractures), and injection fluid properties (flow rate, viscosity, and compressibility) (El Rabaa, 1989; Kumari et al., 2018; Middleton et al., 2015; Qian et al., 2020; Warpinski and Teufel, 1987). Injection of cold water into highly heated rock can result in thermal damage on the rock structure due to induced thermal cracks, which can cause enhancement of flow performance due to new fluid paths or widening of existing fluid paths (Guo et al., 2018; Kumari et al., 2017). Considering hydraulic fracturing under high temperatures, these thermally enhanced flow paths can enhance near-wellbore permeability resulting in higher fluid leak-off to the matrix (Kumari et al., 2018; Stephens and Voight, 1982). Therefore, the stimulation mechanism and the stimulated volume can be different compared to the room temperature condition, and it is essential to understand the underlying mechanisms of the high-temperature hydraulic fracturing process followed by flow enhancement. In this regard, considering the complexity associated with field-scale hydraulic fracturing exercises, laboratory scale hydraulic fracturing experiments, and laboratory-scale permeability experiments can provide valuable information of hydraulic fracturing process followed by flow performance of hydraulically fractured rock under controlled temperature and stress conditions.

A large number of laboratory-scale hydraulic fracturing tests has been performed to understand the effect of in-situ stress, interactions of natural and hydraulic fractures, injection rate, and properties of the injection fluid (Blanton, 1982; Li et al., 2019; Sarmadivaleh, 2012; Wanniarachchi et al., 2017; Warpinski and Teufel, 1987; Zoback et al., 1977). These studies have revealed that hydraulic fracture propagation is strongly stress-dependent such that hydraulic fractures propagate along the major principal stress and the difference of horizontal stresses and the presence of natural fractures determine the geometry and quantity (i.e. either single or multiple) of fractures (Blanton, 1982; Sarmadivaleh, 2012; Zoback et al., 1977). In addition, it has been identified that injection rate, wellbore perforation, the presence of notches and properties of injection fluid influence the breakdown pressure (the pressure at which the rock is fractured) (Fallahzadeh et al., 2015; Wanniarachchi et al., 2017; Zoback et al., 1977). However,

[1] *School of Civil, Mining and Environmental Engineering, University of Wollongong, NSW 2522, Australia. Email: pabasara@uow.edu.au Tel: +61 2 4221 5694*
[2] *Department of Civil Engineering, Monash University, Building 60, Melbourne, Victoria, 3800, Australia. Email: ranjith.pg@monash.edu Tel: +61 3 990 54982*

only a few studies have paid attention to flow enhancement due to laboratory hydraulic fractured samples under different stress conditions. Wanniarachchi et al. (2017) has employed hydraulically fractured siltstone samples under room temperature and found that increase of effective pressure from 4 to 24 MPa at 1 MPa injection pressure results reduction of fracture permeability of 56% and 81% for partially fractured and fully fractured samples, respectively. However, almost all the studies have been performed under room temperature conditions under small in-situ stress conditions, and therefore the effect of temperature on the hydraulic fracturing process is little known.

In this regard, recent experimental work of Kumari et al. (2018), who conducted hydraulic fracturing experiments under a wide range of confining pressures from 0 to 60MPa and temperatures from room temperature to 300°C simulating different geothermal environments, provides an essential understanding of hydraulic fracturing under extreme stress and temperature conditions applicable to the geothermal environment. Continuing that study, the present research aims to understand the flow performance of hydraulically fractured granite rock, which was fractured under high temperature and pressure conditions. Coupled flow mechanical experiments were conducted to study the flow performance of granite specimen, which was hydraulically fractured under 60 MPa confining pressure and two temperature conditions (room temperature and 300 °C). In addition, the effect of rock microstructure on high-temperature fluid injection has been identified through high-resolution CT scanning testing. Therefore, the present study could understand the flow behaviour of hydraulically fractured rock in both micro and mesoscale, which can provide valuable knowledge on underline mechanisms of the flow performance of geothermal reservoir rocks.

EXPERIMENTAL METHOD

Sample Description

Granite samples were collected from the Harcourt Batholith, which is a large multiple intrusion located in Northwest Victoria, Australia. The selected granite had, medium to coarse-grained gran structure, and it was found that it has similar mineralogical and petrographic characteristics of granites found in Australian geothermal wells. **Figure 1** illustrates the closer view of a typical granite specimen. Before the experiments, the samples were carefully characterized in terms of mineral and petrophysical features and, **Table 1** summarizes the petrophysical and mechanical properties of selected granite under room temperature atmospheric conditions.

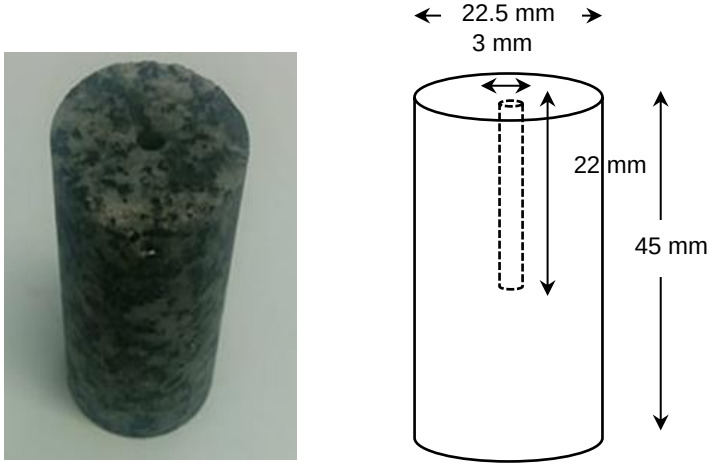

Figure 1: Closer view and a schematic representation of a typical sample prepared for hydraulic fracturing experiments

To prepare the samples for high temperate and high-pressure hydraulic fracturing followed by permeability experiments, cylindrical samples of 22.5mm diameter were prepared employing a low coring rate and water as a lubricant drilling coring process. Then samples were cut into 45 mm lengths, and two ends were carefully ground to ensure perfectly parallel surfaces (surface irregularity > 10 μm). Next, to initiate the hydraulic fracture, a 3mm diameter wellbore was created by drilling the sample centres mid up to mid-depth (22 mm) employing a 3 mm drill bit. In order to minimize sample damage, a low drilling speed was employed with a lubricant and, this created wellbore acted as an axial notch to

aid hydraulic fracture initiation (Sarmadivaleh, 2012). Using the compressed air drill hole was cleaned, and then samples were washed and stored in a 40 °C oven to remove moisture.

Table 1: Physical, and petrographic and mechanical properties of selected granite under room temperature and pressure conditions

Main minerals	Quartz (48%), K-feldspar (10%), plagioclase feldspar (18%), biotite (22%), other minerals (2%)
Grain size distribution	0.3-1.5 mm
Bulk density (kg/m^3)	2630
Porosity (%)	0.8
Uniaxial compressive strength (MPa)	149.5
Young's modulus (GPa)	18.2
Poisson's ratio	0.22
Brazilian tensile strength (MPa)	7.0

High-temperature and high-pressure tri-axial testing apparatus

The recently developed high-temperature and high-pressure tri-axial apparatus available at Deep Earth Energy Laboratory in Monash University (Shao, 2015) was employed for the high-temperature pressure hydraulic fracturing experiments and fracture permeability experiments. This testing apparatus is capable of simulating deep geothermal conditions with confining pressure up to 137 MPa, injection pressure up to 165 MPa, axial load up to 1000kN and temperature up to 300 °C. The laboratory overview and the inside view of the testing machine are shown in **Figure 2**.

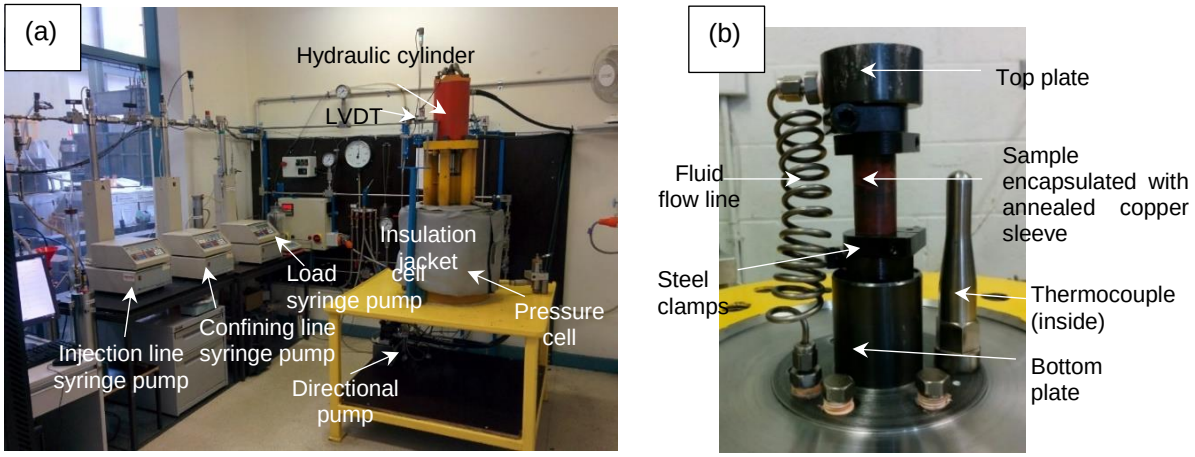

(a) Laboratory overview of the high-pressure high-temperature triaxial set-up (b) Closer view of the inside of the cell

Figure 2: High-pressure high-temperature triaxial set-up

In this system, for fluid injection, applying confining pressure and axial load, three independent hydraulic pumps are used and, an electric band heater has been employed to apply the required temperature. Temperature is carefully controlled and monitored with two independent thermocouples attached to the pressure cell and inside of the pressure cell (**Figure 2(b)**), respectively. Further, the specially designed heating blanket has been used to eliminate any thermal losses during the experiments. In order to produce large confining pressures under high temperatures, silicone oil has been used as the confining medium. Further, to isolate the sample with the confining media, particularly machined annealed copper sleeves are employed as the membrane. Also, specially designed four steel clamps were employed to eliminate any leakages or fluid losses. A bottom pedestal with a top O ring was employed for the hydraulic fracturing experiments, while permeability experiments were conducted with another bottom pedestal with machined distribution rings (Kumari et al., 2018). Specifically manufactured high-temperature O rings made of Teflon were employed for all the high-temperature experiments.

Hydraulic fracturing and fracture permeability test procedure

Throughout all the hydraulic experiments, the axial load was controlled to apply 2 kN of deviatoric force. This ensured larger axial stress compared to confining press which resulted in the initiation of hydraulic fracture along the wellbore. Prior to both hydraulic fracturing experiments, the target temperature and pressure were applied and maintained for 3 hours prior to fluid injection to achieve equilibrium. The

temperature was applied at a heating rate of 5 °C/min to minimize possible damages to the sample due to thermal shock. Considering the limited pump volume of 65 ml and the fluid leak-off through the samples, water was injected employing a constant rate of 5 ml/min. **Table 2** represents the hydraulic fracturing test conditions employed for selected samples considered in this study.

Table 2: Hydraulic fracturing test conditions of each sample

Sample	Confining Pressure (MPa)	Temperature (°C)	Breakdown Pressure (MPa)
1	60	20	72.43
2	60	300	66.41

After the fracturing tests, the copper sleeve was carefully removed by machining it and, fracture permeability tests were conducted with a new membrane. The same high-temperature, high-pressure triaxial set-up was employed for the experiments changing the bottom pedestal. The axial load was maintained throughout all the experiments to apply equal pressure as confining pressure such that $\sigma_1 = \sigma_3$. Drained permeability tests were then performed by injecting distilled water at selected injection pressures under the considered confining pressure and temperature conditions. In order to understand the effect of confining pressure and injection pressure on hydraulically fractured specimens under room temperature and high-temperature conditions, permeability test series were performed at room temperature. The experimental programme was carefully designed to minimize the damage of the fracture asperities such that both confining pressure and injection pressures were increased gradually from lower pressures to higher pressures. Further, it was ensured not to release confining pressure throughout the experiments. Similar to the hydraulic fracturing experiments, all the fluid flow lines were drained prior to the experiment to eliminate the presence of any air bubbles. Accumulating downstream fluid mass was recorded using an electronic balance with an accuracy of 0.01g, and the corresponding steady-state mass flow rate was calculated. The detailed fracture permeability test programme employed in the present study is presented in **Table 3**.

Table 3: Experimental methodology

Sample	Confining Pressure (MPa)	Injection Pressure (MPa)
Sample 1	10	7, 8, 9
	15	12, 13, 14
	20	16, 17, 18, 19
Sample 2	10	4, 5, 6, 8
	20	5, 8, 10,12, 15
	40	10, 20 25, 30, 35
	60	20, 30, 40, 50

CT scanning tests

One of the main aims of this experimental study is to understand the flow performance of hydraulically fractured samples which were fractured under high temperatures. Due to high-temperature conditions, rock micro-structure can certainly be altered. Hence, high-resolution CT scanning imaging technology was employed with Australian Synchrotron to understand the micro-scale effects of rock during high-temperature hydraulic fracturing. The Imaging and Medical beamline (IMBL), which allows 10 µm voxels high resolution, was employed for the scanning process.

RESULTS AND DISCUSSIONS

Breakdown curve of the hydraulic fracturing process

Figure 3 illustrates the pressure-time curve of the hydraulic fracturing process for the two samples. Considering those breakdown pressure curves, four main stages of pressure development stages can be identified: (i) initial pressure development, (ii) linear wellbore pressurization, (iii) hydraulic fracturing, (iv) post-failure stage. It was found that the breakdown pressure is both stress and temperature-dependent. However, stress influence is greater compared to the temperature effect (Kumari et al., 2018).

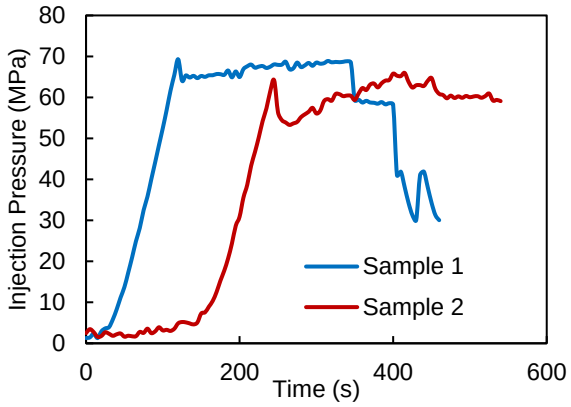

Figure 3: The pressure-time curve for different confining pressures

With increasing confining pressure, breakdown pressure is increased, as discussed in the well-known Hubbert-Wills criteria (Hubbert and Willis, 1957) as follows.

$$P_b - P_0 = 3\sigma_h - \sigma_H + \sigma_T \quad (1)$$

Where P_b is the breakdown pressure, P_o is the initial pore pressure, σ_h is the minimum horizontal stress, σ_H is the maximum horizontal stress, and σ_T is the tensile strength of the rock. It should be noted that the present experimental results are lower than the HW criteria due to the small sample size, unperforated wellbore, which results in a larger pressurization area, and temperature effects.

Further, considering the pressure-time curve, a small initial pressure development time can be identified while that region is considerably higher in Sample 2. During the initial pressurization stage, water is entered to pre-existing fractures and accessible pores resulting in a small pressure development. Once those accessible pores are filled, wellbore pressurization begins resulting in a significant pressure development. However, in the high-temperature experiment, with increasing temperature viscosity of water is linearly decreased while its compressibility is non-linearly increased (Lemmon et al., 2002). Further, cold water injection into the comparatively hot rock can result in the initiation and propagation of thermally induced cracks casing higher fluid leak-off under this condition. This can result in a larger initial pressurization region under high-temperature conditions as well as relatively low breakdown pressure. Further, considering the post-failure stage indicates induction of secondary cracks in Sample 2 can be identified. Larger pressure drops in Sample 1 indicate the release of pressure (releasing water to downstream) along the induced hydraulic fracture; however, the fracture has been closed due to the confining pressure, resulting in a residual pressure equal to the confining pressure. This feature is less evident in Sample 2, instead of irregular small pressure drops and rises can be identified. This suggests that due to the thermal effect, the fracturing mechanism under high temperate is different from room temperature due to the alteration of rock structure and fracturing fluid properties.

Effect of temperature on hydraulic fracturing process

In order to understand the effect of rock microstructure due to the high-temperature hydraulic fracturing process, high-resolution CT imaging technology was employed, and **Figure 4** illustrates CT images taken from the cross a cross-section (1 mm away from the wellbore) of each sample. Considering the CT images, it should be noted that the dark colour regions indicate low-density regions (voids and fracture) while light colour regions indicate high-density regions (different minerals).

Considering CT images of Sample 1, a tiny single hydraulic fracture is visible, closer to the injection point; however, with increasing sample length (away from the injection point), induced hydraulic fracture aperture has been decreased. Reduction of fracture aperture during fracture propagation can be explained as a reduction of free energy during fracture propagation. However, compared to the room temperature experiments, under the considered resolution (10 μm), fracture aperture is hardly visible in Sample 2, which was fractured under 300 °C. Interestingly, as shown in **Figure 4(b)**, the enlarged images show a porous region closer to the wellbore, which indicates damage to the rock microstructure due to the injection of cold water into the hot rock. It should be noted that both Sample 1 and 2 were performed under the same confining pressure; therefore, this microstructural alteration solely depends on the temperature effect. The high-temperature hydraulic fracturing process has resulted in the

induction of micro-cracks in the wellbore zone apart from the main fracture due to the quenching effect. Further, the breakdown pressure curve of the high-temperature experiment suggests that these secondary cracks are further initiated and propagated during the continuous injection of cold water. However, compared to the main fracture aperture, these secondary fractures are relatively low (< 20 µm). Although the apertures of thermally induced fractures are considerably lower than the main hydraulic fracture aperture due to the higher fracture density, these induced secondary fractures may enhance the flow performance of the sample. For example, compared to the room temperature condition, measured main fracture aperture (hydraulically induced) at the inlet location under 300 °C is 50% smaller, which might be due to the viscosity reduction of the fluid-induced under high temperature and enhanced fluid leak-off due to thermal damage (Li et al., 2021; Middleton et al., 2015). Therefore, in order to understand their flow performance, independent drain permeability tests were conducted over a wide range of stress conditions, as discussed in the next section.

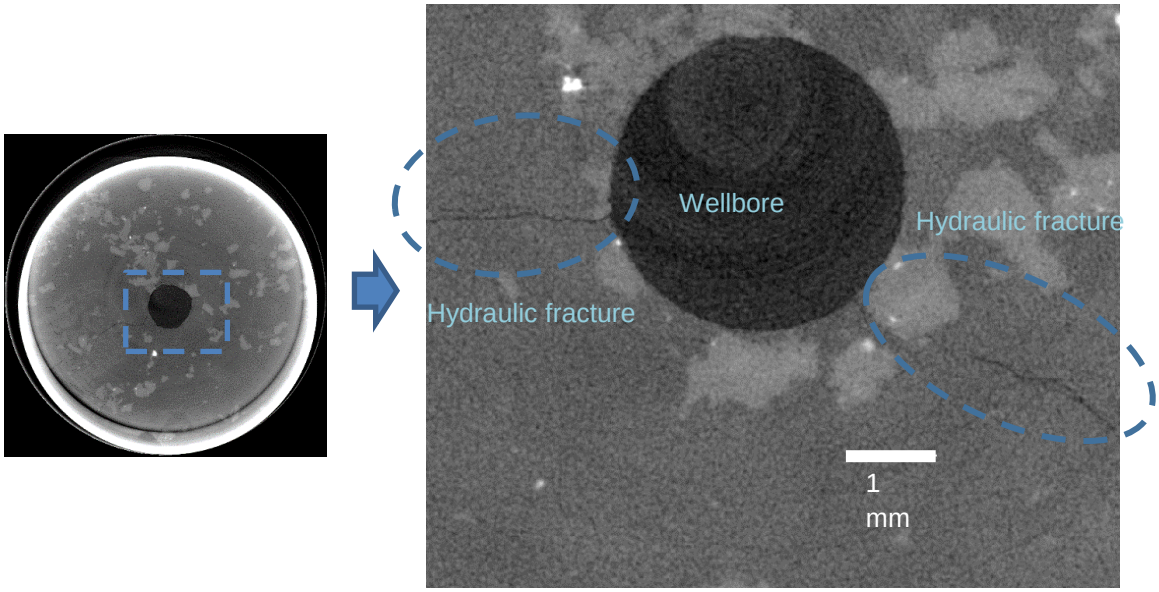

(a) Sample 1

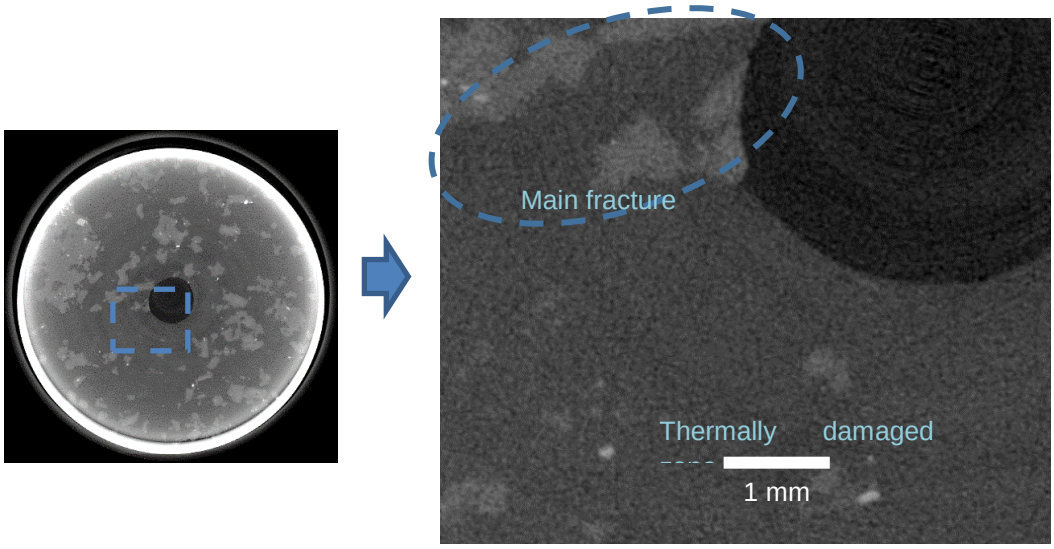

(b) Sample 2

Figure 4: Enlarge views of CT images

Steady-state flow rate of the hydraulically fractured granite

Flow behaviour of Sample 1 (which was hydraulically fractured under 60 MPa confining pressure and room temperature) and Sample 2 (which was hydraulically fractured under 60 MPa confining pressure and 300 °C) were investigated over a wide range of confining pressures (σ_c) and different injection pressures (σ_i) at room temperature condition. It was ensured that $\sigma_i < \sigma_c$ to ensure further hydraulically

induced fractures do not initiate during the experiment by eliminating any negative effective stress development. The detailed test programme employed for both samples is presented in **Table 3**.

Considering the extreme injection pressures employed, first, the applicability of Darcy law (Darcy, 1856) for the present experimental conditions were checked, and **Figure 5** illustrates the variation of steady-state flow rate with injection pressure for both samples. For all the confining pressures, the steady-state flow rate was increased with increasing the injection pressure. A linear relationship with the coefficient of determination (R^2) over 0.9 in all the considered conditions was found. Further, the calculated highest volumetric flow rate was 1.6 x10^{-10} m^3/s (For 10 MPa confining pressure and 9 MPa injection pressure in Sample 2). Therefore, laminar flow condition, Darcy law was employed to calculate the permeability of the fractured rocks.

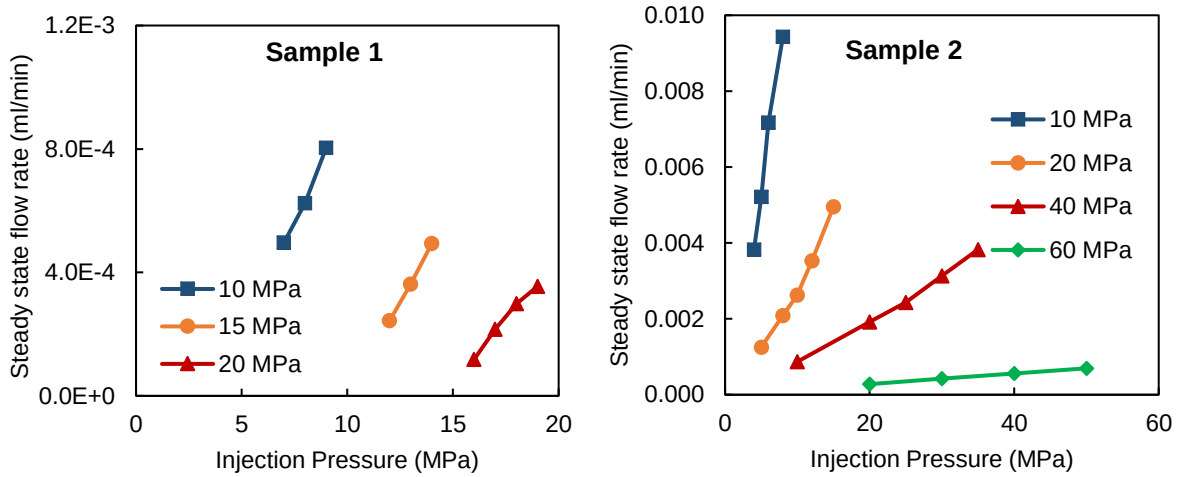

Figure 5: Steady-state flow rate with injection pressure for different confining pressures

Permeability of the hydraulically fractured granite

Considering the selected granite type under 10 MPa confining pressure and 8 MPa injection pressure, the steady-state volumetric flow rate of the intact sample was found as 1×10^{-13} m^3/s. However, under the same condition, this figure for both Sample 1 and 2 was 1×10^{-11} m^3/s and 1.6×10^{-10} m^3/s, respectively. Therefore, throughout the study, permeability was calculated, neglecting matrix permeability with the assumption that fluid flow only occurs through the induced fracture as follows.

Neglecting the gravitational effects, Darcy law for one-dimensional flow can be expressed as follows:

$$Q = -\frac{Ak}{\mu}\frac{dP}{dx} \tag{2}$$

where Q is the volumetric flow rate, A is the free flow area, k is the permeability of the media, μ is the dynamic viscosity of the fluid, and dP is the pressure drop along the distance dx.

In order to obtain the free flow area, it is important to incorporate fracture aperture for hydraulically fractured samples and hence assuming fracture flow occurs through two idealized parallel plates, fracture permeability was calculated based on the cubic law as suggested by Witherspoon et al. (1980) as follows:

$$Q = -\frac{we^3}{12\mu}\frac{dP}{dx} \tag{3}$$

where e is the hydraulic aperture and w is the fracture width.

Therefore, assuming linear pressure gradient, hydraulic fracture aperture can be calculated for the present condition as:

$$e = \left(\frac{12\ Q\mu}{w}\frac{L}{P_i - P_o}\right)^{1/3} \quad (4)$$

where L is the sample length P_i is the injection pressure, and P_o is the outlet pressure.

Further, considering free flow area as; $A = ew$ and, combining Eq. 6 and 7, fracture permeability for each condition can be calculated as follows:

$$k = \frac{e^2}{12} \quad (5)$$

where k is the permeability of the fracture.

Figure 6 illustrates the variation of calculated permeability with injection pressure for both Sample 1 and 2.

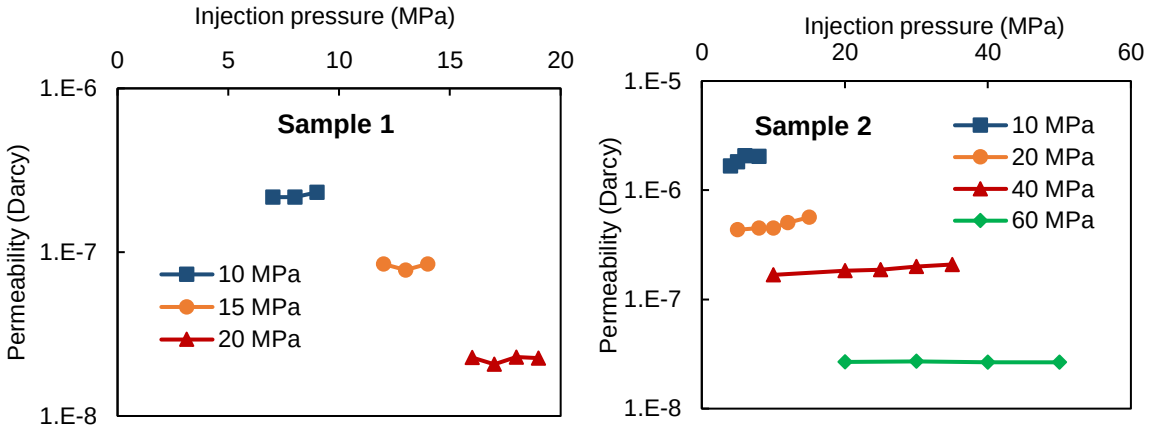

Figure 6: Permeability variation with injection pressure for different confining pressures

It was found that with increasing confining pressure, both steady-state flow rate and permeability non-linearly decrease in both Samples. Interestingly it was found that both the steady-state flow rate and permeability of Sample 1 is considerably lesser than Sample 2. For example, under 10 MPa confining pressure and 8 MPa injection pressure steady-state flow rate of Sample 1 was 1 x10^{-11} m^3/s, while this was 1.6 x10^{-10} m^3/s in Sample 2, which is one order higher than Sample 1. Under this condition, permeability reduction was also in the same order, such that 0.21 mD permeability was found in Sample 1 while this figure was 2 mD in Sample 2. It should be noted that, because of the smaller flow rate of Sample 1, flow-through experiments were conducted under comparatively small confining pressures (up to 20 MPa) and under higher injection pressures (minimizing the effective stress). Considering the present experimental work, since both Samples were hydraulically fractured under the same confining pressure by employing identical stress conditions effect of temperature on the hydraulic fracturing process can be captured.

As identified in the CT images, only a single hydraulic fracture is present in Sample 1, while Sample 2 is consisted of multiple fractures in the wellbore zone due to injection of cold water into the hot rock. Although the fracture aperture of both main fracture and the secondary fractures of Sample 2 is considerably low (secondary fracture apertures are < 20 µm while main fracture aperture is 50% lower than the Sample 1, because of the creation of perforated zone closer to the wellbore zone, the porosity of Sample 2 is considerably higher than Sample 1. This was evident with a higher leak-off during the hydraulic fracturing process also. Therefore, permeability is almost one order higher in the sample hydraulically fractured under high temperatures under the same stress conditions. As a result of the injection of cold water into the hot rock, due to the induced thermal stresses, rock microstructure can be altered with the induction of both intergranular and intragranular cracks depending on the temperature condition. Considering the present experiment, cold water was injected into the granite rock which was under 300 °C during the hydraulic fracturing experiments. Therefore induction of intergranular cracks alone quartz-quartz, quartz-feldspar boundaries can be expected as identified in (Isaka et al., 2018). These thermally induced cracks can substantially alter the flow performance of the rock matrix

(Ghassemi and Kumar, 2007; Kumari et al., 2018) and therefore, considering the geothermal context, induction of multiple thermally induced fractures can be expected, which results in considerable permeability enhancement of near-wellbore zone.

The effect of stress state on flow characteristics of fractured granite

While linear increment of steady-state flow rate was observed with increasing injection pressure, calculated permeability change was insignificant in a certain confining pressure. However, with increasing confining pressure, it was found that both steady-state flow rate and permeability was non-linearly decreased, depicted in **Figures 5-7**.

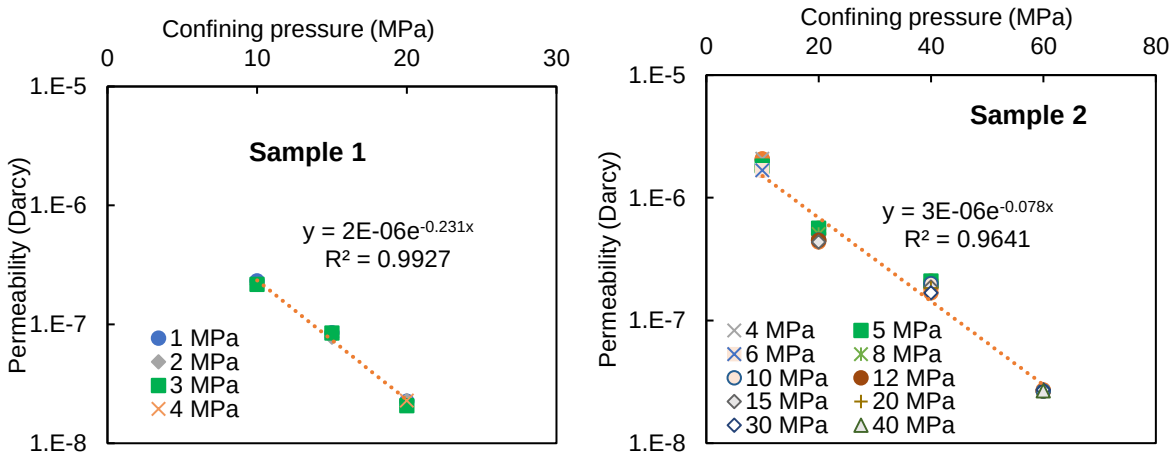

(a) Permeability variation with confining pressure of the two samples under different effective stresses

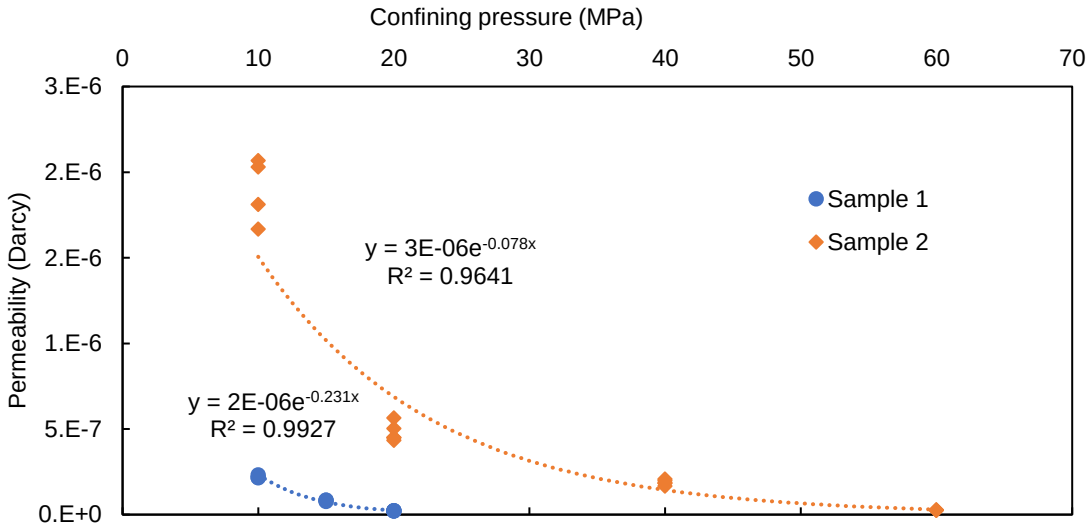

(b) Comparison of permeability variation of two samples for different effective stresses

Figure 7: Effect of the stress state on fracture permeability

For example, considering Sample 1, the average steady-state flow rate decreased from 1x10-11 m3/s to 4x10-12 m3/s once the confining pressure increased from 10 MPa to 20 MPa. The respective permeability reduction was also in the same order, such that from 0.22 mD to 22 nD. However, considering Sample 2, it was found that the average steady-state flow rate was decreased from $1x10^{-7}$ m^3/s from $5x10^{-10}$ m^3/s once the confining pressure is increased from 10 MPa to 60 MPa. The respective permeability reduction was also in the same order, such that from 1.8 mD to 0.18 mD. Further, it was found that the flow performance of each sample due to applied stress levels was also dissimilar. For example, once confining pressure increased from 10 MPa to 20 MPa, the respective permeability

reduction of Sample 1 was one order while that figure was 75% in Sample 2. It further emphasizes that the induced fractures (both hydraulically and thermally) are highly stress-dependent such that increased normal stress results in non-linear closure of those fractures. Since Sample 1 consists of one single fracture, the effect of normal stress is more significant because once the single fracture is closed, the entire flow is impeded. However, since Sample 2 has consisted of multiple fractures, the fluid flow tends to take preferential perforated paths under higher stress conditions resulting in better flow performance.

The corresponding stress state significantly influences the flow performance of both intact and fractured rocks. In this regard, change of both normal stress (confining pressure P_c) and pore pressure (injection pressure P_e) plays critical roles (Makurat et al., 1991; Rutqvist and Stephansson, 2003). Therefore, the stress condition acting on the sample is generally discussed with the term effective stress:

$$P_e = P_c - \alpha P_i \tag{6}$$

where α is taken to be 1.0 for water (Cheng, 2014). Therefore, permeability variation with increasing confining pressure was checked under different effective stresses, as shown in **Figure 7**. It was found that the permeability of both samples was exponentially decreased. This result is consistent with a number of studies that employed different types of intact rocks. This implies that with increasing reservoir depth/ reduction of pore pressure, a non-linear relationship (exponential/logarithmic) can be employed to understand the flow performance of hydraulically stimulated reservoir rocks (Rutqvist and Stephansson, 2003). With the increment of effective pressure on the fractured reservoir, the flow resistance increased as a result of the closure of the induced aperture (Tuncay and Corapcioglu, 1995). Therefore, it can be identified that, under high confining pressures (deep reservoir conditions), once the pore pressure is realized during the hydraulic fracturing process, the induced fracture is substantially closed. This can result in a significant reduction of transport characteristics, and therefore it is essential to keep the fracture open once the fluid pressure is released. In this regard, proppants which are typically small solid particles (sand, ceramic), chemical or gel (Patel et al., 2014), are generally mixed to the fracturing fluid in the oil and gas fields. Considering high-temperature geothermal environments, it is important to evaluate the performance of different proppant types (Gomaa et al., 2015), and this can be identified as a future research direction.

CONCLUSIONS

In this study, the flow performance of hydraulically fractured granites under two different temperature conditions was investigated. From the study results, the following conclusions are drawn:

- Under high temperatures, the mechanism of the hydraulic fracturing process is different compared to room temperature conditions due to thermal damage to the rock matrix and the change of material properties of the fracturing fluid.
- CT images confirmed that one single fracture is induced at room temperature. However, a perforated zone with multiple inter-crystalline cracks is induced in the wellbore zone apart from the main fracture under the high-temperature hydraulic fracturing process.
- Although the fracture aperture of both main fracture and the thermally induced fractures are relatively low compared to the room temperate condition, because of the creation of perforated zone closer to the wellbore zone, experimental results revealed permeability is almost one order higher in the sample hydraulically fractured under high temperature under the same stress conditions up to 20 MPa confining pressure.
- It was identified that non-linear reduction in fracture permeability due to applied normal stresses. Further reduction of effective stress on the fracture resulted in an increment of fluid discharge due to associated pore pressure variations and an increase of fracture aperture.

REFERENCES

Blanton, T.L., 1982. An experimental study of interaction between hydraulically induced and pre-existing fractures, SPE Unconventional Gas Recovery Symposium. Society of Petroleum Engineers.

Cheng, A.H.-D., 2014. Fundamentals of poroelasticity. Analysis and Design Methods: Comprehensive Rock Engineering: Principles, Practice and Projects, 113.

Darcy, H., 1856. Les fontaines publiques de la ville de Dijon: exposition et application. Victor Dalmont.

El Rabaa, W., 1989. Experimental study of hydraulic fracture geometry initiated from horizontal wells, SPE Annual Technical Conference and Exhibition. Society of Petroleum Engineers.

Fallahzadeh, S., Rasouli, V. and Sarmadivaleh, M., 2015. An investigation of hydraulic fracturing initiation and near-wellbore propagation from perforated boreholes in tight formations. Rock Mechanics and Rock Engineering, 48(2): 573-584.

Ghassemi, A. and Kumar, G.S., 2007. Changes in fracture aperture and fluid pressure due to thermal stress and silica dissolution/precipitation induced by heat extraction from subsurface rocks. Geothermics, 36(2): 115-140.

Gomaa, A., Gupta, D. and Carman, P., 2015. Viscoelastic Behavior and Proppant Transport Properties of a New High-Temperature Viscoelastic Surfactant-Based Fracturing Fluid, SPE International Symposium on Oilfield Chemistry. Society of Petroleum Engineers.

Guo, L.-L., Zhang, Y.-B., Zhang, Y.-J., Yu, Z.-W. and Zhang, J.-N., 2018. Experimental investigation of granite properties under different temperatures and pressures and numerical analysis of damage effect in enhanced geothermal system. Renewable Energy, 126: 107-125.

Hubbert, M.K. and Willis, D.G., 1957. Mechanics Of Hydraulic Fracturing. Society of Petroleum Engineers.

Isaka, B.L.A., Gamage, R.P., Rathnaweera, T.D., Perera, M.S.A., Chandrasekharam, D. and Kumari, W.G.P., 2018. An influence of thermally-induced micro-cracking under cooling treatments: mechanical characteristics of Australian granite. Energies, 11(6): 1338.

Kumari, W., Ranjith, P., Perera, M., Chen, B. and Abdulagatov, I., 2017. Temperature-dependent mechanical behaviour of Australian Strathbogie granite with different cooling treatments. Engineering Geology, 229: 31-44.

Kumari, W., Ranjith, P., Perera, M., Li, X., Li, L., Chen, B., Isaka, B.A. and De Silva, V., 2018. Hydraulic fracturing under high temperature and pressure conditions with micro CT applications: geothermal energy from hot dry rocks. Fuel, 230: 138-154.

Lemmon, E.W., Huber, M.L. and McLinden, M.O., 2002. NIST reference fluid thermodynamic and transport properties–REFPROP. NIST standard reference database, 23: v7.

Li, B.Q., da Silva, B.G. and Einstein, H., 2019. Laboratory hydraulic fracturing of granite: Acoustic emission observations and interpretation. Engineering Fracture Mechanics, 209: 200-220.

Li, N., Zhang, S., Wang, H., Ma, X., Zou, Y. and Zhou, T., 2021. Effect of thermal shock on laboratory hydraulic fracturing in Laizhou granite: An experimental study. Engineering Fracture Mechanics, 248: 107741.

Makurat, A., Barton, N., Rad, N. and Bandis, S., 1991. Joint conductivity variation due to normal and shear deformation. Publikasjon-Norges Geotekniske Institutt, 182: 1-6.

Middleton, R.S., Carey, J.W., Currier, R.P., Hyman, J.D., Kang, Q., Karra, S., Jiménez-Martínez, J., Porter, M.L. and Viswanathan, H.S., 2015. Shale gas and non-aqueous fracturing fluids: Opportunities and challenges for supercritical CO_2. Applied Energy, 147: 500-509.

Patel, P., Robart, C., Ruegamer, M. and Yang, A., 2014. Analysis of US Hydraulic Fracturing Fluid System and Proppant Trends, SPE Hydraulic Fracturing Technology Conference. Society of Petroleum Engineers.

Qian, Y., Guo, P., Wang, Y., Zhao, Y., Lin, H. and Liu, Y., 2020. Advances in laboratory-scale hydraulic fracturing experiments. Advances in Civil Engineering, 2020.

Rutqvist, J. and Stephansson, O., 2003. The role of hydromechanical coupling in fractured rock engineering. Hydrogeology Journal, 11(1): 7-40.

Sarmadivaleh, M., 2012. Experimental and numerical study of interaction of a pre-existing natural interface and an induced hydraulic fracture, Curtin University.

Shao, S., 2015. Coupled Thermo-Hydro-Mechanical (THM) Behaviour of Rock Relevant to the Geothermal Industry (Doctoral dissertation), Monash Univerisity.

Stephens, G. and Voight, B., 1982. Hydraulic fracturing theory for conditions of thermal stress. International Journal of Rock Mechanics and Mining Sciences and Geomechanics Abstracts, 19(6): 279-284.

Tuncay, K. and Corapcioglu, M.Y., 1995. Effective stress principle for saturated fractured porous media. Water Resources Research, 31(12): 3103-3106.

Wanniarachchi, W.A.M., Gamage, R.P., Perera, M.S.A., Rathnaweera, T.D., Gao, M. and Padmanabhan, E., 2017. Investigation of depth and injection pressure effects on breakdown pressure and fracture permeability of shale reservoirs: an experimental study. Applied Sciences, 7(7): 664.

Warpinski, N. and Teufel, L., 1987. Influence of geologic discontinuities on hydraulic fracture propagation (includes associated papers 17011 and 17074). Journal of Petroleum Technology, 39(02): 209-220.

Witherspoon, P.A., Wang, J.S., Iwai, K. and Gale, J.E., 1980. Validity of cubic law for fluid flow in a deformable rock fracture. Water resources research, 16(6): 1016-1024.

Zoback, M., Rummel, F., Jung, R. and Raleigh, C., 1977. Laboratory hydraulic fracturing experiments in intact and pre-fractured rock. International Journal of Rock Mechanics and Mining Sciences and Geomechanics Abstracts, 14(2): 49-58.